Robotica (2022), **40**, pp. 102–119
doi:10.1017/S0263574721000412

CAMBRIDGE
UNIVERSITY PRESS

RESEARCH ARTICLE

Development of nonmotorized mechanisms for lower limb rehabilitation

Rogério S. Gonçalves and Lucas A. O. Rodrigues*

Faculty of Mechanical Engineering, Federal University of Uberlândia, Uberlândia, Brazil
*Corresponding author. Email: lucas.ep@outlook.com

Received: 19 March 2020; **Revised:** 23 March 2021; **Accepted:** 25 March 2021; **First published online:** 4 May 2021

Keywords: Closed kinematic chains, Geometrical matrix method, Lower limb, Rehabilitation, Singularity analysis.

Abstract

This paper concerns with the development of three nonmotorized individual lower limb joints rehabilitation mechanisms based on a four-bar linkage, and mechanical movement transmission from the motion of the patient's upper limb. Initially, mathematical and computational models are built based on the desired angular motions for the hip, knee, and ankle. A prototype for the knee mechanism was constructed for initial experimental tests. The first test with wooden mannequin show that this prototype is lightweight, has an output movement compatible with the amplitudes, is easy to build and operate, being thus ready for clinical tests with healthy and impaired subjects.

1. Introduction

Robotics has a wide field of applications, which includes the therapeutic robots that aids patients with movement impairments in the rehabilitation process such as stroke patients [1, 2, 3]. Stroke is considered as one of the most frequent causes of deaths in Europe and the United States of America [4].

There are several types of rehabilitation robots, based on different therapy methods and kinematic designs, and their applications can bring benefits to the rehabilitation process such as the reduction of active labor force, as well as the expansion of the range of continuous motion passive therapy [5, 6, 7, 8, 9].

Although the research of clinical robotic structures tends to applications using electrical and pneumatic actuators, there are advantages for designing these structures that only use the input/force of the own user. The main advantage of a passive structure relies on the reduction of high initial investment required for clinics and hospitals to apply rehabilitation structures in poststroke patient's treatment[11].

Therefore, in this work, the procedures of the development of a nonmotorized structure able to contribute to the accessibility of rehabilitation structures is presented. The main contribution of this paper is to demonstrate the feasibility of a low-cost passive structure in an instrument to assist the rehabilitation of poststroke patients.

The idea of exploring passive self-operated systems in poststroke rehabilitation as an alternative treatment like the one presented in this work is present in recent literature. For example, some rehabilitation devices have been presented without the use of conventional inputs such as DC motors, servos, and pneumatic actuators. Soares Jr [10] proposed an exoskeleton using crank-rocker linkages and cams to convert a cycling motion input from the user's upper limbs to the human gait movement on the user's lower limbs.

A nonmotorized structure based on a cam linkage was recently proposed to aid treadmill gait rehabilitation [12]. Its design includes a two degree of freedom seven-bar crank-slider system, achieving the

human foot trajectory by using inverse kinematics. Computational simulations of this design show a good match with the desired trajectory, although no prototype of this structure has yet been built.

Some passive commercial ankle orthosis and prostheses can aid patients to achieve a normal gait movement on this joint. However, this equipment is designed for overground gait purposes, and works only for low-speed walking. Examples of nonmotorized robots for upper limbs like Dampace [13] and T-Wrex (Armeo) [14] can be found in the literature.

Cho and Song [15] presented results of feedback training using a nonmotorized upper limb rehabilitation structure by showing positive effects on upper extremity kinematic performance of chronic stroke survivors.

Therefore, the main objective of the structures presented in this paper is to explore the same benefits of the previously mentioned researches, while applying a simple yet efficient mechanical design to reduce the setup, operational, and maintenance costs and keep the structures easy to use.

Recent research also shows that a neural coupling mechanism between both limbs, noted on combined movements of the human body, for example, the arms and legs synchronous movements during gait and cooperative hand movements while writing on a keyboard [16, 17, 18]. The neuronal connection between the upper and lower limbs is still being studied, but recent results have revealed that the coupling of both limbs during rehabilitation exercises can enhance the recovery of the patients.

The use of a cycling ergometer with an arm and a leg on cyclical exercises was able to assist the recovery of poststroke patients [19], and there is also evidence that cycling exercises on both limbs, as intended in this work, improves walking and interlimb integrity in chronic stroke [20]. This type of training works with different kinematics when compared with gait exercises but activates similar neural networks on the brain [21].

Recent rehabilitation structures are also applying indirect action methods on the paretic limbs to stimulate active muscular motion. There are works based on cable-driven actuators for upper and lower limb rehabilitation [22, 23, 24, 25, 26] and pelvic actuation on a body weight support to provide gait assistance [27]

Additionally, to the best knowledge of the authors, no other nonmotorized structures for lower limb rehabilitation have been presented. Based on these facts, this paper concerns with the design of three novel inexpensive structures for lower limb exercises. Some evidence of self-operated device application in the treatment of lower limb impairments positive effects is described in ref. [28] like psychosocial and functional benefits, which improve patients' lives. The use of self-operated systems also helps the patients to build independence, improving their motivation and self-esteem, and contributing to a more autonomous life [16].

Furthermore, nonmotorized rehabilitation mechanisms can be a more affordable solution on rehabilitation devices once the material requirements for building this equipment are low-cost and easy to find [11]. In this paper, a design for the novel nonmotorized mechanisms are proposed based on the classical four-bar linkage, using a method for singularity analysis of closed kinematic chains. A conceptual model of one of the mechanisms and the prototype built are shown in Fig. 1.

Thus, the potential contributions of this paper are summarized in Table 1.

2. Lower limb movements

To develop the project of the mechanisms, it is necessary to understand the correct ranges of each movement on the human lower limb joints. The amplitudes of these movements will be used as the output parameter during the mathematical modeling phase of the mechanism's development. Ref. [29] shows that the human movements of the lower limbs can be referenced using three planes, which is defined as transversal, frontal, and sagittal planes, as shown in Fig. 2. The position of the individual shown in Fig. 2 is known as the anatomical position, which defines the zero degrees reference for all the movements of the lower limb.

https://doi.org/10.1017/S0263574721000412 Published online by Cambridge University Press

Table 1. *Contributions expected for the proposed nonmotorized structures.*

Benefit	Principle explored
Amplify the field of appliance	Apply inexpensive materials and design in the solution [11]
Assist the recovery process	High-insensitivity interlimb cycling exercises [16, 17, 18, 20]
Stimulate functional independence	Self-operated rehabilitation mechanisms [28, 16]

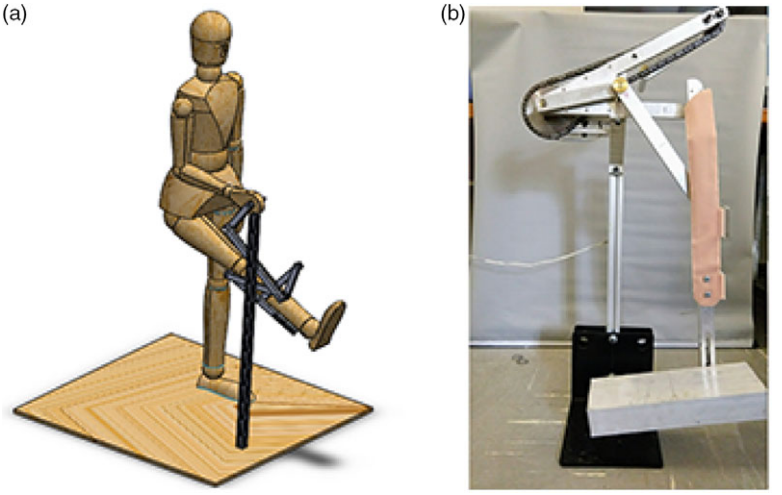

Figure 1. *(a) Conceptual model of the nonmotorized rehabilitation mechanism for the knee and (b) the prototype built for experimental tests.*

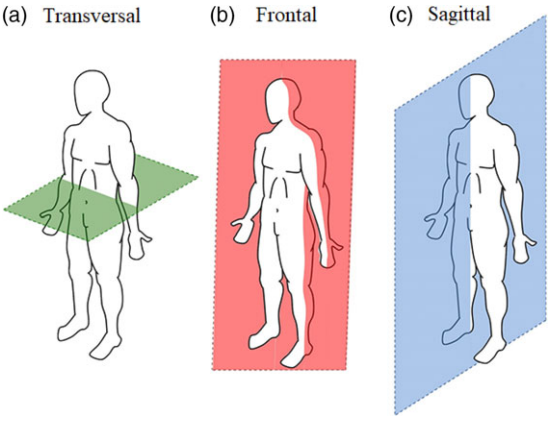

Figure 2. *Notation adopted for the human body movement planes: (a) the transversal plane; (b) the frontal plane; and (c) the sagittal plane.*

The elemental movements that compose all the mobility of the lower limb are defined, including the gait, as they occur in the hip, knee, and ankle joints. The notation used for each movement is its angular amplitude, in degrees. Since the structures developed in this work are plane structures, the elemental movements of the sagittal plane can provide exercises for the main movements applied to the human gait. Further information on other movements can be found in ref. [29].

https://doi.org/10.1017/S0263574721000412 Published online by Cambridge University Press

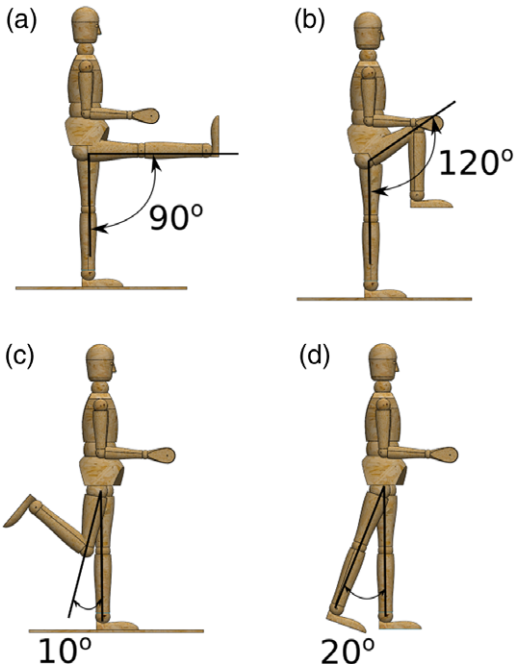

Figure 3. *Movements of the hip on the sagittal plane: Flexion phase movements with (a) knee at anatomical position and (b) with full flexion knee; extension phase movements with (c) knee at full flexion and (d) at anatomical position.*

2.1. Hip movements

The hip joint of the human body is responsible for one's locomotion and body lift [29]. It has three Degrees of Freedom (DOF), allowing angular movements along the three axes, which makes the hip behaves like a spherical mechanical joint.

The basic movements of the hip are defined as abduction–adduction, on the frontal plane, flexion–extension, on the sagittal plane, and longitudinal rotation, which occurs on the longitudinal axis of the limb [29].

Although all the basic movements of this joint have important roles in the human gait, the flexion–extension movement is detailed due to the application of the proposed mechanisms. The flexion–extension movement is the displacement of the leg around the transversal axis, defined by the intersection of the transversal and frontal planes [29].

On the flexion phase, the leg displaces forwards, allowing the contact of body and thigh. The position of the knee directly influences the maximum amplitude of this movement, being approximately 0–90° when the knee is in the anatomical position, as shown in Fig. 3(a), and 0–120° when the knee is full flexion, as shown in Fig. 3(b).

These values are known as the active flexion. There are higher amplitudes when the limb is affected by external efforts, for example, pulling the leg against the body results in a 145° displacement. These extended amplitudes are called passive flexion [29].

The extension phase brings the leg backward of the frontal plane, and has a smaller amplitude, being 0–10° with the knee on flexion, Fig. 3(c), and 0–20° with the extended knee, Fig. 3(d) [29]. In this paper, only the active amplitudes were accounted for the output parameter of the proposed mechanism, aiming to deal only with the range where the patients should move the limb by themselves.

https://doi.org/10.1017/S0263574721000412 Published online by Cambridge University Press

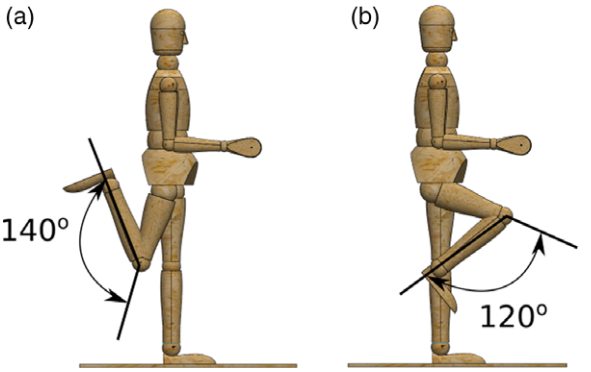

Figure 4. *Movements of the knee on the sagittal plane with (a) hip on flexion and (b) hip on extension.*

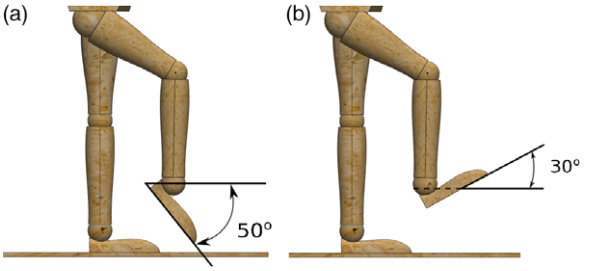

Figure 5. *Movements of the ankle on the sagittal plane:(a) flexion phase and (b) extension phase.*

2.2. Knee movements

The knee is the intermediate joint of the human lower limb with two DOF. The main movement, called flexion–extension, allows the subject to regulate the distance between its body and the ground. The second DOF occurs only while the knee is on flexion and it is responsible for the foot rotation and will not be explored on the devices designed for this work to keep its simplicity and focus on the treatment of the main movement of this joint [22]. The flexion phase of the knee movement is defined as the sagittal movement able to displace the back of the leg toward the back of the thigh. Ranges of this movement can vary depending on the hip position. For a previous hip extension, it goes from 0° to 120°, Fig. 4(a), and 0° to 140° if the hip is on flexion, Fig. 4(b) [29].

Extension movements, defined as the opposite phase of the flexion, usually occurs only as a passive movement on the knee, with little amplitudes smaller than 5° [29]. As mentioned before, only the active range of each joint mobility was considered, which are represented in Figs. 3 and 4.

2.3. Ankle movements

In the joint of the ankle, two DOF can be defined as the movements of abduction–adduction, and flexion–extension, with similar characteristics to the previous joints. The abduction–adduction movement occurs in the frontal plane, displacing the foot from the sagittal plane, while the flexion–extension movement displaces the foot from the frontal plane to the sagittal plane [29].

Unlikely hip and knee, the flexion–extension movement of the ankle does not allow a passive range of displacement. Therefore, flexion phase of this movement goes from 0° to 30°, Fig. 5(a), and extension phase from 0° to 50°, Fig. 5(b), without the influence of external efforts.

https://doi.org/10.1017/S0263574721000412 Published online by Cambridge University Press

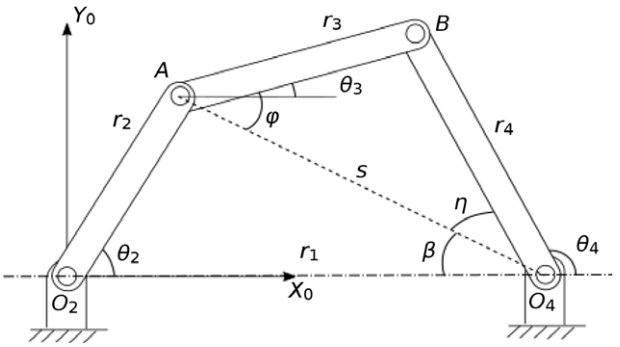

Figure 6. *Notation for bars and angles of a four-bar linkage.*

With all amplitudes of each joint of the human lower limb properly defined, its limits are used as the workspace for the mechanisms of this paper to ensure correct movements during exercises with the equipment.

3. Mathematical model

To design the process of these rehabilitation devices, the first step is to choose a suitable mathematical model to represent the mechanics of the structures in a generic perspective. A mechanism can be defined as a physical system able to transform an input movement into another output [30].

Following this definition, the goal of the structures proposed in this paper is to convert a complete revolution of a crank from the upper limb of a patient to an angular oscillatory movement, designed to fit the lower limb joints amplitude. Therefore, a well-defined system known as the four-bar linkage can be applied as a fundamental model for this work.

Mechanisms defined as a four-bar linkage have their behavior as a system defined by the Grashof's law, dividing them into three groups: Crank-rocker, double-rocker, and double-crank [30].

According to the desired behavior for the mechanisms proposed (where a continuous angular motion is converted on a bounded angular motion) matches the characteristics of the crank-rocker four-bar linkage.

3.1. Algebraic method

The analysis of the crank-rocker linkage is done utilizing a method based on geometrical relations of the bars, where its inner angles and its respective bar lengths are related. To create a reference system for the procedure applied on this method, let the bars and angles of a four-bar linkage be stated as described in Fig. 6.

Since the system is defined as a crank-rocker linkage, the angle θ_2 is designed to reach 360° of rotation, and the angle θ_4 must match the angular amplitude of the according lower limb joint. The specified angles for the lower limb joints are based on the sum of the amplitudes of flexion and extension movements as defined in Section 2.

For the ankle, a flexion of 30° combined with an extension of 50° results in an 80° total amplitude. For the knee, considering the hip extension position, there is a 120° amplitude from the flexion. Finally, for the hip, considering the knee at 0°, 20° of extension sums with 90° of flexion, obtaining a total amplitude of 110°. Passive amplitudes of the hip and knee, and the small knee extension were not included in operational range of the mechanisms.

The geometrical relations, Fig. 6, that can define the mathematical model are obtained using the Cosines law as presented in (1)–(4). The inverse cosine can be applied as described on the equations

https://doi.org/10.1017/S0263574721000412 Published online by Cambridge University Press

Table 2. *Bar lengths obtained for each mechanism.*

Joint of mechanism	r_1 (mm)	r_2 (mm)	r_3 (mm)	r_4 (mm)
Ankle	280	104	235	164
Knee	280	140	263	162
Hip	273	260	235	164

since the angular range of the bars is limited between 0 and π rad. Therefore, the angles described do not reach discontinuities of the inverse cosine function.

$$s = \left(r_1^2 + r_2^2 - 2r_1 r_2 \cos\theta_2\right)^{1/2} \tag{1}$$

$$\beta = \cos^{-1}\left[\left(r_1^2 - r_2^2 + s^2\right) / (2sr_1)\right] \tag{2}$$

$$\varphi = \cos^{-1}\left[\left(r_3^2 - r_4^2 + s^2\right) / (2sr_3)\right] \tag{3}$$

$$\eta = \cos^{-1}\left[\left(r_4^2 - r_3^2 + s^2\right) / (2sr_4)\right] \tag{4}$$

Thus, applying the previous relations, it is possible to obtain the angles θ_3 and θ_4, as shown in (5)–(8).

$$\theta_3 = \varphi - \beta \qquad 0 \le \theta_2 < 180^\circ \tag{5}$$

$$\theta_3 = \varphi + \beta \qquad 180^\circ \le \theta_2 < 360^\circ \tag{6}$$

$$\theta_4 = 180^\circ - \eta - \beta \qquad 0 \le \theta_2 < 180^\circ \tag{7}$$

$$\theta_4 = 180^\circ - \eta + \beta \qquad 180^\circ \le \theta_2 < 360^\circ \tag{8}$$

Therefore, the equations presented before can be applied as a tool to obtain the length of bars r_1, r_2, r_3, r_4 that converts correctly the angular input θ_2 into the angular output θ_4. This is done with the aid of a differential evolution algorithm, which varies values for each bar until relations (1)–(4) be satisfied [26, 31]. The values of the variables are chosen by the algorithm with respect to constraints built based on the Eqs. (1)–(8). The obtained mechanisms are designed to suit persons with heights up to 1.80 m.

Although the angular output θ_4 of the mechanisms are designed to match the entire amplitude of each joint of the lower limb, the structure allows patients to perform movements in both directions, for instance, clockwise and counterclockwise on the crank. Thus, patients that are unable to perform the complete flexion–extension movements can operate the mechanisms with oscillatory movements in order to generate a comfortable angular output for the injured limb.

Thus, the obtained mechanisms would fit for up to 95% of the Brazilian population, scope of the future clinical trials. Additionally, the chosen height constraint also ensures that prototypes of the mechanisms are fit for the wooden puppet applied on the first experimental test.

The evolutional algorithm interacted with a population of 60 length individuals with lengths bounded on lateral limits, varying from 100 to 500 mm, and different transversal sections, based on commercial and easy to find profiles. The optimization converges to the minimal lengths that would not violate any of the geometrical constraints defined on Eqs. (1)–(8). The algorithm also includes the singularity analysis and the stress equations, described in Sections 3.2 and 3.4, as constraints that should not be violated along with the workspace of each mechanism. Thus, the resulting design is expected to be free of singularities and with a maximum stress compatible with the chosen section.

The obtained lengths are shown in Table 2.

With the lengths described in Table 2, all the positions can be calculated for any input θ_2 using the geometrical relations (1)–(4). Hereafter, the position data of the conversion of the input angle θ_2 into the output θ_4 is calculated for a complete revolution of crank with a resolution of 1°, which is then applied to the static model of the structure.

https://doi.org/10.1017/S0263574721000412 Published online by Cambridge University Press

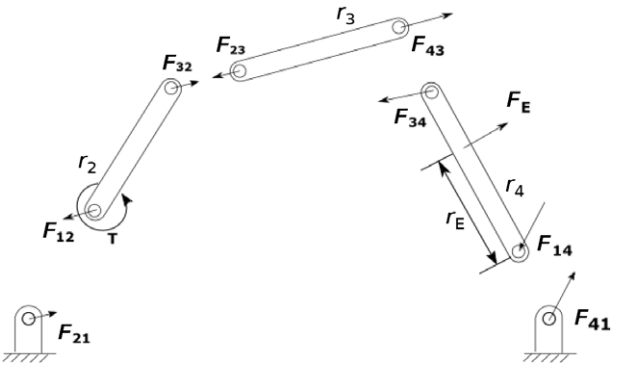

Figure 7. *Free-body diagram of four-bar linkage with an input torque T and an external force F_E representing the weight of patients limb.*

3.2. Static model

On this kind of rehabilitation structure, low values for speed and acceleration are applied during the physical therapy exercises. Thus, a static model can be utilized to obtain the stress on each bar of the mechanism on all calculated positions, to specify the transversal section of each bar. By using a static model, it is possible to obtain a smaller and simpler model for the structure, easing the modeling process.

The structures are expected to operate on a low-speed application with the highest frequency close to 0.2 Hz. A dynamic study of the structures was also performed considering the deformation and inertia of the bars applying a finite elements analysis (FEA) and building the Frequency Response Function (FRF) along with the entire workspace, and obtaining the first five natural frequencies and modes with a relative error smaller than 0.1%.

The FRF showed no significant differences between the static response and the operational maximum frequency. Therefore, the static Newton–Euler approach presented in this section is valid.

The inertial reference frame of all mechanisms is represented by $O_2X_0Y_0$, Fig. 6, and the sum of angular momentum is calculated in relation to points O_2, A, and O_4. The fundamental static conditions, described in (9)–(11), are applied on each bar of the mechanism, considering a free-body diagram, as shown in Fig. 7.

$$\Sigma F_x = 0 \tag{9}$$

$$\Sigma F_y = 0 \tag{10}$$

$$\Sigma M_z = 0 \tag{11}$$

Grouping up the obtained equations, a matrixial form can be constructed to represent the equilibrium of the entire system, as shown in (12).

$$[A]\{F\} = \{B\} \tag{12}$$

In the free-body diagram, forces coming from a bar i into a bar j are represented by vectors F_{ij}. Force F_E is an external force considering the mechanical impedance coming from the lower limb of the patient, with a single point connection between bar r_4 and the limb orthosis. Force F_E can have a generic direction, but as it represents the weight of the lower limb of the patient, it was considered to be always vertical. Torque T represents the angular input from the upper limb into the crank bar of the mechanism.

To represent the forces for the entire system with a matrixial form, let vector $\{F\}$ be forces F_{ij} with projections on X_0 and Y_0, resulting in an equilibrium matrix A, and vectors $\{F\}$ and $\{B\}$, as shown in (13).

https://doi.org/10.1017/S0263574721000412 Published online by Cambridge University Press

Table 3. *External loads for each mechanism.*

Joint of mechanism	Mass proportion (%)[32]	Total load (N)	Safety factor (N)
Ankle	1.5	22.07	33.01
Knee	5.8	85.35	128.02
Hip	16.3	239.85	359.78

$$\begin{bmatrix} -1 & 0 & 1 & 0 & 0 & 0 & 0 & 0 & 0 \\ 0 & -1 & 0 & 1 & 0 & 0 & 0 & 0 & 0 \\ 0 & 0 & -r_2 \sin\theta_2 & r_2 \cos\theta_2 & 0 & 0 & 0 & 0 & 1 \\ 0 & 0 & 1 & 0 & 1 & 0 & 0 & 0 & 0 \\ 0 & 0 & 0 & 1 & 0 & 1 & 0 & 0 & 0 \\ 0 & 0 & 0 & 0 & -r_3 \sin\theta_3 & r_3 \cos\theta_3 & 0 & 0 & 0 \\ 0 & 0 & 0 & 0 & 1 & 0 & -1 & 0 & 0 \\ 0 & 0 & 0 & 0 & 0 & 1 & 0 & -1 & 0 \\ 0 & 0 & 0 & 0 & -r_4 \sin\theta_4 & r_4 \cos\theta_4 & 0 & 0 & 0 \end{bmatrix} \begin{pmatrix} F_{12_x} \\ F_{12_y} \\ F_{32_x} \\ F_{32_y} \\ F_{43_x} \\ F_{43_y} \\ F_{14_x} \\ F_{14_y} \\ T \end{pmatrix} = \begin{pmatrix} 0 \\ 0 \\ 0 \\ 0 \\ 0 \\ 0 \\ -F_{E_x} \\ -F_{E_y} \\ r_E \sin\theta_4 F_{E_x} - r_E \cos\theta_4 F_{E_x} \end{pmatrix} \tag{13}$$

To determine the correct load F_E coming from the lower limb, an estimated value is taken based on mean human proportions [32] as described in Table 3. The load is calculated by taking the normal fraction of body mass of each part of the lower limb. The entire lower limb mass is considered for the hip mechanism, while the knee mechanisms consider the lower leg and foot relative mass, and the ankle takes into account only the foot mass. As mentioned before, the structures must fit for 95% of the Brazilian population, which means that the external load must consider individuals with height up to 1.80 m and weight up to 150 kg [33].

An oblong hole was also featured on bar r_4, as presented in Fig. 8, to allow position adjustments of the contact point. The hole is positioned after the joint between bars r_3 and r_4 on the knee and hip mechanism, and between the joints of the bar r_4 on the ankle mechanism.

Solving Eq. (12) considering external force F_E for positions of θ_2 between 0° and 360°, all forces F_{ij} and the required input torque T can be obtained. The obtained values components are then utilized to calculate stress on transversal section of all bars.

The sections are specified considering stress coming from the normal direction, σ_{Ni}, and from the bending momentum, σ_{Bi}. Equations (14)–(16) defines the calculation of the total stress on each bar transversal section, where A_i represents the area of transversal section of the i-th bar, I_i is the respective

https://doi.org/10.1017/S0263574721000412 Published online by Cambridge University Press

Table 4. *Calculated stress and selected transversal sections of bars.*

Joint of mechanism	Stress on bars (MPa) r_1	r_2	r_3	r_4	Transversal section (width/height/thickness) (mm)
Ankle	0.86	0.93	1.02	18.6	12.7 × 25.4 × 2
Knee	23.6	23.6	23.8	230.4	12.7 × 25.4 × 3
Hip	8.2	8.2	8.4	214.9	25.4 × 25.4 × 5

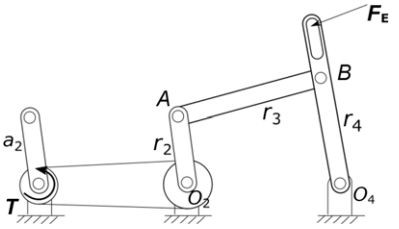

Figure 8. *A complete scheme of the mechanisms design, including the oblong hole on bar r_4 (knee or hip case), and the chain drive for torque transmission (T).*

inertia momentum, and d_i is the distance between the point of maximum bending stress and the neutral line of bar i.

$$\sigma_{Ni} = \frac{F_{xi}\cos\theta_2}{A_i} + \frac{F_{yi}\sin\theta_2}{A_i} \tag{14}$$

$$\sigma_{Fi} = \frac{F_{xi}\sin\theta_2 d_i}{2I_i} + \frac{F_{yi}\cos\theta_2 d_i}{2I_i} \tag{15}$$

$$\sigma_{ri} = \sigma_{Ni} + \sigma_{Fi} \tag{16}$$

The transversal sections of the bars are then selected applying an differential evolution algorithm similar to the previously utilized on the bar length specification. The limit of stress on each bar is considered 276 MPa, as specified for 6061 T6 aluminum alloys [34]. The algorithm evaluated different values for A_i, d_i, and I_i based on common commercial profiles in order to keep a high availability of the applied materials.

A safety factor equal to 2 on all stress calculations was also applied to ensure that mechanism bars will resist any unmodelled parameters that may affect the systems during operation.

The obtained maximum stress values of the bars and the selected transversal sections applying the differential evolution algorithm are shown in Table 4.

3.3. Chain drive system

To facilitate the operation of the structures by the user, a load compensation system is applied to the mechanisms. A chain drive system was selected, based on the available materials. Other solutions may be applied like the use of springs and counterweights.

This chain drive will serve to adjust the position of the upper limb during the transmission of the angular input from patients arm to bar r_2. In addition, the relation between the gears will allow a reduction in the input torque of the upper limb, which will keep the required effort at a comfortable level. A scheme of the complete mechanism is shown in Fig. 8.

The level of comfort to operate the structures correctly can be determined based on the proportion of the human arm and maximum torque measures, which is found to be around 71 Nm for males and

https://doi.org/10.1017/S0263574721000412 Published online by Cambridge University Press

Table 5. *Torque transmission and analysis.*

Joint	Maximum torque (Nm)	Torque limit (Nm)	Chain drive reduction
Ankle	3.8241	16.5	1
Knee	38.7391	16.5	2.8174
Hip	78.5580	16.5	5.9514

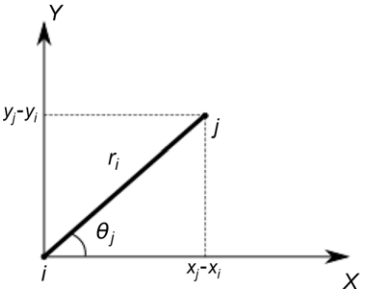

Figure 9. *Geometrical relations of an elementary bar with length of r_i and angle θ_j.*

33 Nm for females [35]. In this paper, 50% of the female mean torque is applied as the limit for the mechanisms, obtaining the values displayed in Table 5.

The chain drive reduction, Table 5, is generated applying calculated reductions on proportions between gears. A third gear is also applied to ensure correct tension on the chain.

3.4. Singularity analysis

Singularities are positions of closed-chain mechanisms that may cause local control methods to fail [36]. To guarantee the correct design of mechanisms, it is necessary to evaluate all the positions on its workspace to find if it reaches singular positions.

Singularity analysis on serial manipulators is usually solved using the Jacobian Matrix [36, 37]. Since the four-bar linkage is a closed kinematic chain, the method purposed in refs. [37, 38, 39] is selected for analysis of the rehabilitation mechanisms designs.

First, let the position of a bar r_i be defined as described in Fig. 9. From this definition, it is possible to write the relations (17) and (18).

$$r_i \cos\theta_j = x_j - x_i \tag{17}$$

$$r_i \sin\theta_j = y_j - y_i \tag{18}$$

Multiplying (17) by $\cos\theta_j$ and (18) by $\sin\theta_j$, and summing the results, it is obtained as

$$r_i = (x_j - x_i)\cos\theta_j + (y_j - y_i)\sin\theta_j \tag{19}$$

Rearranging in a matrixial form, (19) can be written as

$$r_i = \{x_i \;\; y_i \;\; x_j \;\; y_j\} \begin{pmatrix} -\cos\theta_j \\ -\sin\theta_j \\ \cos\theta_j \\ \sin\theta_j \end{pmatrix} = \{x_e\}^T \{h\} \tag{20}$$

https://doi.org/10.1017/S0263574721000412 Published online by Cambridge University Press

where $\{x_e\}$ represents the vector coordinates of nodes *i,j* that defines bar r_i. Squaring the bar lengths, it is possible to represent it as described in (21) and shortened in (22).

$$r_i^2 = \{x_i \;\; y_i \;\; x_j \;\; y_j\}$$

$$\begin{bmatrix} \cos^2\theta_j & \cos\theta_j \sin\theta_j & -\cos^2\theta_j & -\cos\theta_j \sin\theta_j \\ \cos\theta_j \sin\theta_j & \sin^2\theta_j & -\cos\theta_j \sin\theta_j & -\sin^2\theta_j \\ -\cos^2\theta_j & -\cos\theta_j \sin\theta_j & \cos^2\theta_j & \cos\theta_j \sin\theta_j \\ -\cos\theta_j \sin\theta_j & -\sin^2\theta_j & \cos\theta_j \sin\theta_j & \sin^2\theta_j \end{bmatrix} \begin{pmatrix} x_i \\ y_j \\ x_j \\ y_j \end{pmatrix} \tag{21}$$

$$r_i^2 = \{x_e\}^T [G_e] \{x_e\} \tag{22}$$

Matrix $[G_e]$ is called elementary geometrical matrix of bar *i* and has a null matrixial product with its velocity vector $\{\dot{x_e}\}$ [37, 38, 39]. This relation is stated in (23).

$$[G_e]\{\dot{x}_e\} = \{0\} \tag{23}$$

Equation (23) represents a linear system of equations related to the velocity of nodes *i,j*. It must be written for all bar elements of the mechanism.

Let *n* be the number of nodes that compose the linkage. The number of nodal coordinates of a plane mechanism is equal to 2*n*. Thus, a vector $\{x\}$ grouping all nodal coordinates of the linkage is described as

$$\{x\} = \{x_1 \;\; y_1 \;\; x_2 \;\; y_2 \;\; \cdots \;\; x_n \;\; y_n\}^T \tag{24}$$

Then, the elementary geometrical matrix can be expanded to all the nodal coordinates, as shown in (25).

$$\{r^2\} = \{x\}^T [\overline{G_e}] \{x\} \tag{25}$$

Therefore, a mechanism with n elements has its elementary geometrical matrix defined by

$$\begin{gathered} [\overline{G}_{e_1}]\{\dot{x}\} = \{0\} \\ [\overline{G}_{e_2}]\{\dot{x}\} = \{0\} \\ \vdots \\ [\overline{G}_{e_n}]\{\dot{x}\} = \{0\} \end{gathered} \tag{26}$$

Summing up the *n* elementary geometrical matrix on the expanded form, the global geometrical matrix $[G]$ is obtained, as described in (27) and (28).

$$[G]\{\dot{x}\} = \{0\} \tag{27}$$

where

$$[G] = \sum_{e=1}^{n} [\overline{G}_e] \tag{28}$$

Finally, constraints of the fix nodes and node duplication must be unconsidered to simplify the global geometrical matrix.

Once the matrix [G] is calculated for all the positions of the mechanisms workspace, singularity analysis procedures can be applied.

To find positions that may be singular, this method seeks for variations on the number of DOF of the system [37, 38, 39]. This is done solving (27) as an eigenproblem, as in (29), finding $\{v_i\}$ eigenvectors and λ eigenvalues.

$$[G]\{\dot{x}\} = \lambda\{\dot{x}\} \tag{29}$$

https://doi.org/10.1017/S0263574721000412 Published online by Cambridge University Press

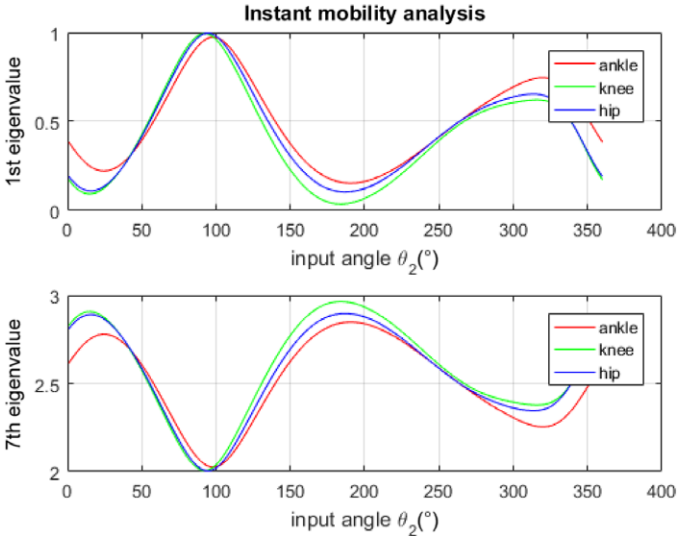

Figure 10. *Results of the nonzero eigenvalues analysis of ankle, knee, and hip mechanisms.*

One can note that (27) is a case of (29) and the Jacobian matrix. The number of DOF of a mechanism in a single cycle defined as f can be obtained with its mobility analysis [37, 38, 39].

The l eigenvectors $\{v_i\}$ corresponding to λ null eigenvalues are linearly independent vectors that describe the motion of the mechanism. Thus, these l eigenvectors correspond to f DOF of the mechanism. This means that if, at any position in the cycle of motion, the number of the l eigenvectors changes, there will be a singularity in this position.

Also, if at any point of the cycle, the eigenvectors corresponding to the inputs or the outputs of the mechanism shows linear dependency, the system will have a singularity due to dependent inputs or outputs.

The methodology presented is applied computationally on all positions of the designed structures, with a resolution of 1°.

After calculating the global geometrical matrix $[G]$, and solving the eigenproblem in (29) for all structure designs, it is clear that, while other eigenvalues remain constant, only the first and the seventh eigenvalues change their values along the cycle of motion, regardless of the target joint.

According to the criteria specified for the eigenvalues, none of these eigenvalues should reach zero in any position of the cycle. Otherwise, the mechanism will pass on a singular position. For all three proposed designs, the first and seventh eigenvalues did not reach a null value in any of the analyzed positions. This can be noted by observing the graphics of value variation of these eigenvalues, as shown in Fig. 10.

The eigenvectors obtained from each position of the mechanisms were analyzed, finding that there was no linear dependency on the inputs and the outputs. The absence of these dependencies combined with the constancy of the nonzero eigenvalues leads the analysis to conclude that the designed mechanisms are non-singular for the analyzed workspace.

4. Computational simulations and experimental tests

4.1. CAD/CAE models and simulations

Before the construction of the physical model for experimental tests was build the CAD/CAE models of each structure and submit then to simulations of the complete cycle of motion.

https://doi.org/10.1017/S0263574721000412 Published online by Cambridge University Press

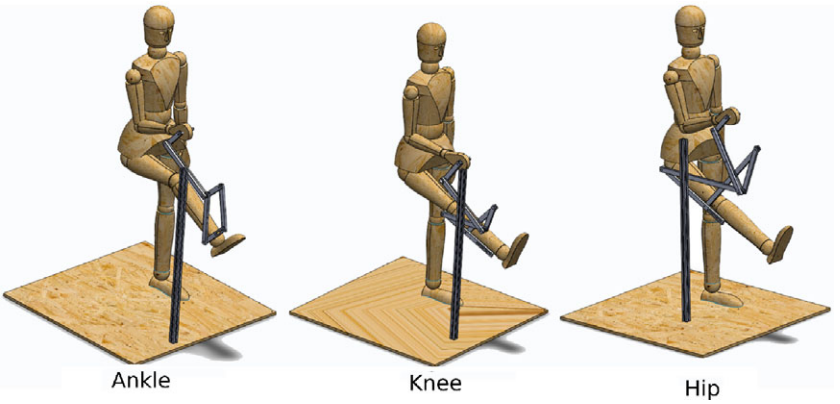

Figure 11. *Complete CAD models of ankle, knee, and hip mechanisms, connected with the lower limb of an anthropometrical wooden puppet.*

To simulate the movement of the structures, a 3D model of an anthropometrical wooden puppet was applied, as displayed in Fig. 11.

All simulations include the input movements on the crank, which is transmitted to the four-bar linkage through the chain drive and shows the output movement of bar r_4 acting directly on puppet's lower limb.

A sequence of obtained simulations is shown in Fig. 12, for ankle, knee, and hip joints, respectively.

4.2. Experimental tests

The built prototype is shown in Figs. 1(b) and 13(a). A basic adjustable stand was included for mechanism positioning. Additionally, a rotary encoder sensor was inserted and applied to generate data and integrate the structures with electronic serious games in future work.

The first experimental test was a measurement of the full amplitude of the angular output of the prototype. It was made by attaching the inclinometer to the lower limb of the wooden dummy, connected to the free extremity of bar r_4 through a leg orthosis, and calculating the variation between the anatomic position of the knee, and its maximum flexion, measuring each position 10 times. This test resulted in an amplitude of $108.8 \pm 1.6°$ (mean $\pm$ std. deviation).

To validate the movement patterns obtained in computer simulations, a simple prototype is constructed based on the specified dimensions on Section 3 for the knee setup, displayed in Fig. 1, and submitted it to three tests: an amplitude measurement done with a digital inclinometer; a continuous motion test while attached to a wooden puppet; and an interface test to integrate the structure with a computer game developed. The game test is a work in progress and will be detailed in future work.

Results make clear that the built prototype has a good repeatability, as the standard deviation is low, and had a shorter amplitude than the projected. This error may occur due to variations on bars lengths, misalignments on screws, and connective mechanical elements between the bars and between the leg orthosis and the output bar.

Next, an operational test was made to evaluate the mobility and ease to use of the structure. During this test, the lower limb of the wooden puppet stays connected to the structure using the same leg orthosis, while a volunteer turns the crank continuously.

The structure was operated for 5 min continuously with a minimum effort from the volunteer to spin the crank. There were no noises from the structure and no difference on efforts between the clockwise and the counterclockwise direction of the crank, leaving it up to the patient to choose which direction it wants to operate the device.

https://doi.org/10.1017/S0263574721000412 Published online by Cambridge University Press

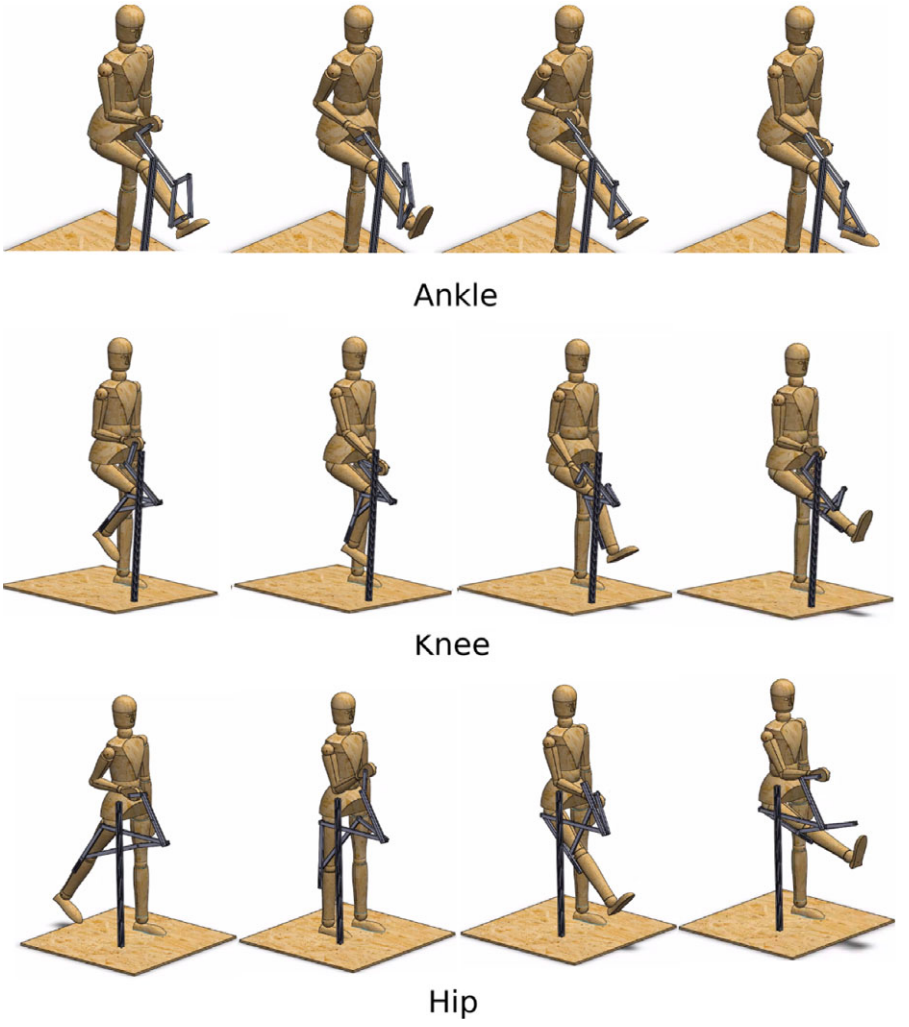

Figure 12. *Sequence of images representing the simulation of the cycle of motion of ankle, knee, and hip mechanisms.*

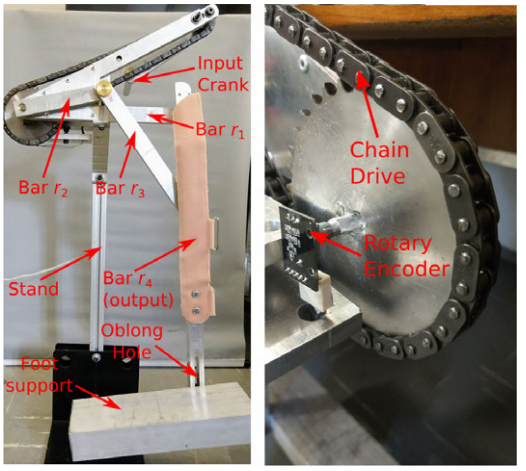

Figure 13. *Built prototype knee mechanism.*

https://doi.org/10.1017/S0263574721000412 Published online by Cambridge University Press

Another important highlight on the test is the possibility to use only a specific range of the structure motion by inverting the crank direction, allowing patients with lower mobility to take advantage of exercising with this structure too.

The video footage of the experimental tests and the computational simulations presented on this paper can be accessed in:
https://tinyurl.com/passiveStructures.

5. Conclusion

In this paper, the importance of research and development of novel rehabilitation structures are presented, highlighting the advantages of self-operating, nonmotorized systems. The proposed designs are simple and were able to reproduce the complete angular amplitude of flexion–extension movements of all joints of the lower limb, separately.

The majority of the lower limb rehabilitation devices use serial and/or parallel structures based on complex mechanical and control systems. The appliance of a simple and well-known mechanism to obtain the desired angular amplitude for the lower limb and stimulating the self-operation by the patients can help to reduce building costs as long while keeping the safety.

The designs were obtained using a complete and fast mathematical model, including a singularity analysis based on an alternative method, which is efficient to closed-chain structures, a quasi-static analysis, and a differential evolution optimization algorithm. Based on the results of this model, it is clear that the mechanisms can be built using light and easy to find materials, reducing costs. Furthermore, the use of a chain drive transmission system was able to allow the operation of the mechanisms requiring minimum efforts.

CAD/CAE simulations show that the mobility of each configuration is compatible with the flexion–extension movements of lower limb joints, confirming that the proposed designs can be able to perform rehabilitation exercises.

A prototype of the knee configuration was built and integrated with an electronic interface using a rotary encoder and a microcontroller and experimental tests were conducted in order to compare computational and experimental data. Amplitude experimental tests show good repeatability and relative error that can be compensated improving the building process of the structures.

Continuous motion experimental tests confirm the pattern observed on simulations and highlights the simple operation, low noise level, and the possibility to work with partial amplitudes and reverse direction of the crank.

With the positive results obtained from the prototype first test, clinical trials of the knee mechanism on healthy and injured patients are being scheduled in order to obtain clinical results to confirm the capability of therapeutically exercise the lower limb of patients.

The next step of this work is the integration of the prototype with a serious game developed to work with inputs from the movement. The game will also register the movement patterns and generate statistical data of each patient, helping health professionals to keep track of improvements and behaviors of the patients.

Acknowledgments. The authors thank the Federal University of Uberlndia and the Brazilian Government Research and Development Departments FAPEMIG, CNPq, and CAPES- Finance Code 001 for the partial financial support to this work.

References

[1] E. D. Oña Simbaña, P. Sanchez-Herrera Baeza, A. Jardon Huete and C. Balaguer, "Review of automated systems for upper limbs functional assessment in neurorehabilitation," *IEEE Access* **7**, 32352–32367 (2019). doi: 10.1109/ACCESS.2019.2901814

[2] W. Hu, G. Li, Y. Sun, G. Jiang, J. Kong, Z. Ju and D. Jiang, "A Review of Upper and Lower Limb Rehabilitation Training Robot," *Intelligent Robotics and Applications* (2017) pp. 570–580.

[3] P. Lum, D. Reinkensmeyer, R. Mahoney, W. Z. Rymer and C. Burgar, "Robotic devices for movement therapy after stroke: Current status and challenges to clinical acceptance," *Top. Stroke Rehabil.* **8**(4), 40–53 (2002).
[4] D. Lackland, Heart Disease and Stroke Statistics 2017 Update A Report From the American Heart Association (2017).
[5] I. Diaz, J. J. Gil and E. Sanchez, "Lower-limb robotic rehabilitation: Literature review and challenges," *J. Rob.* **2011**(11), e759764 (2011).
[6] A. Esquenazi and M. Talaty, "Robotics for lower limb rehabilitation", *Phys. Med. Rehabil. Clin. North Am.* **30**(2), 385–397 (2019). doi: 10.1016/j.pmr.2018.12.012
[7] H. Wang, W. Li, H. Liu, J. Zhang and S. Liu, "Conceptual design and dimensional synthesis of a novel parallel mechanism for lower-limb rehabilitation," *Robotica* **37**(3), 469–480 (2019). doi: 10.1017/S0263574718001121
[8] D. Cafolla, M. Russo and G. Carbone, "CUBE, a cable-driven device for limb rehabilitation," *J. Bionic Eng.* **16**(3), 492–502 (2019). doi: 10.1007/s42235-019-0040-5
[9] S. Viteckova, P. Kutilek, G. de Boisboissel, R. Krupicka, A. Galajdova, J. Kauler, L. Lhotska and Z. Szabo, "Empowering lower limbs exoskeletons: State-of-the-art," *Robotica* **36**(11), 1743–1756 (2018). doi: 10.1017/S0263574718000693
[10] R. Sales Gonçalves, G. Soares and J. C. Carvalho, "Conceptual design of a rehabilitation device based on cam-follower and crank-rocker mechanisms hand actioned," *J. Brazilian Soc. Mech. Sci. Eng.* **41**(3), 277 (2019).
[11] K. Lo, M. Stephenson and C. Lockwood, "The economic cost of robotic rehabilitation for adult stroke patients: a systematic review," *JBI Database Syst. Rev. Implementation Rep.* **17**(4), 520–547 (2019). doi: 10.11124/JBISRIR-2017-003896
[12] Y. Shao, Z. Xiang, H. Liu and L. Li, "Conceptual design and dimensional synthesis of cam-linkage mechanisms for gait rehabilitation," *Mech. Mach. Theory* **104**(2016), 31–42 (2016).
[13] A. Stienen, E. E. G. Hekman, F. van der Helm, G. Prange, M. Jannink, A. Aalsma and H. Kooij, "Dampace: Dynamic Force-Coordination Trainer for the Upper Extremities," *2007 IEEE 10th International Conference on Rehabilitation Robotics*, (c) (2007) pp. 820–826.
[14] R. J. Sanchez, J. Liu, S. Rao, P. Shah, R. Smith, T. Rahman, S. C. Cramer, J. E. Bobrow and D. J. Reinkensmeyer, "Automating arm movement training following severe stroke: Functional exercises with quantitative feedback in a gravity-reduced environment," *IEEE Trans. Neural Syst. Rehabil. Eng.* **14**(3), 378–389 (2006).
[15] K. H. Cho and W.-K. Song, "Feedback training using a non-motorized device for longterm upper extremity impairment after stroke: a single group study," *J. Phys. Ther. Sci.* **28**(2), 495–499 (2016).
[16] S. Sasada, T. Tazoe, T. Nakajima, G. Futatsubashi, H. Ohtsuka, S. Suzuki, E. Paul Zehr and T. Komiyama, "A common neural element receiving rhythmic arm and leg activity as assessed by reflex modulation in arm muscles," *J. Neurophysiol.* **115**(4), 2065–2075 (2016).
[17] J. E. Balter and E. P. Zehr, "Neural coupling between the arms and legs during rhythmic locomotor-like cycling movement," *J. Neurophysiol.* **97**(2), 1809–1818 (2007).
[18] H. J. Huang and D. P. Ferris, "Neural coupling between upper and lower limbs during recumbent stepping," *J. Appl. Physiol.* **97**(4), 1299–1308 (2004).
[19] T. Klarner, T. S. Barss, Y. Sun, C. Kaupp, P. M. Loadman and E. P. Zehr, "Exploiting interlimb arm and leg connections for walking rehabilitation: A training intervention in stroke," *Neural Plast.* **2016** (2016). Article ID 1517968. doi: 10.1155/2016/1517968
[20] C. Kaupp, "Rhythmic Arm Cycling Training Improves Walking and Interlimb Integrity in Chronic Stroke *Master Thesis* (University of Victoria, 2018) p. 105.
[21] E. P. Zehr, J. E. Balter, D. P. Ferris, S. R. Hundza, P. M. Loadman and R. H. Stoloff, "Neural regulation of rhythmic arm and leg movement is conserved across human locomotor tasks," *J. Physiol.* **582**(1), 209–227 (2007).
[22] R. S. Gonçalves, J. C. M. Carvalho, J. F. Ribeiro and V. V. Salim, "Cable-driven robot for upper and lower limbs rehabilitation," *Handb. Res. Adv. Rob. Mechatron.* **2015**, 284–315 (2014). doi: 10.4018/978-1-4666-7387-8.ch011
[23] A. M. Barbosa, J. C. M. Carvalho and R. S. Gonçalves, "Cable-driven lower limb rehabilitation robot," *J. Braz. Soc. Mech. Sci. Eng.* **40**(5), 1–11 (2018). Article ID 245.
[24] R. S. Gonçalves, J. C. M. Carvalho, L. A. O. Rodrigues and A. M. Barbosa, "Cable-driven parallel manipulator for lower limb rehabilitation," *Appl. Mech. Mater.* **459**, 535–542 (2013). doi: 10.4028/www.scientific.net/amm.459.535
[25] T. Alves, M. Chaves D'Carvalho and R. Sales Gonçalves, "Assist-as-needed control in a cable-actuated robot for human joints rehabilitation," *J. Mech. Eng. Biomech.* **3**(5), 57–62 (2019).
[26] R. S. Gonalves, J. C. M. Carvalho and F. S. Lobato, "Design of a robotic device actuated by cables for human lower limb rehabilitation using self-adaptive differential evolution and robust optimization," *Biosci. J.* **32**(6), 1689–1702 (2016).
[27] R. S. Gonalves and L. A. O. Rodrigues, "Development of a Novel Parallel Structure for Gait Rehabilitation," **In:** *Handbook of Research on Advanced Mechatronic Systems and Intelligent Robotics* (2019) p. 4281.
[28] H. Bateni and B. E. Maki, "Assistive devices for balance and mobility: Benefits, demands, and adverse consequences," *Arch. Phys. Med. Rehabil.* **86**(1), 134–145 (2005).
[29] I. Kapandji, *Physiology of the Joints: Lower Limb*, 6th ed. (Churchill Livingstone, London, 2010).
[30] J. J. Uicker, G. R. Pennock, J. E. Shigley and J. M. McCarthy, "Theory of machines and mechanisms," *J. Mech. Des.* **125**(3), 650 (2003).
[31] F. S. Lobato, V. Steffen Jr and L. C. Oliveira-Lopes, "An Evolutionary Approach Based on Search Chaotic Pattern Associated to Differential Evolution Algorithm," *17° Simpísio do Programa de Pós-graduação em Engenharia Mecânica* (2007) p. 9.

[32] C. E. Clauser, J. T. McConville, J. W. Young and C. E. Clauser, Weight, Volume and Center of Mass of Segments of the Human Body. AMRL Technical Report, Wright Patterson Air Force Base, Ohio (1969) pp. 101.
[33] IBGE - Instituto Brasileiro de Geografia e Estatística, Antropometria e Estado Nutricional no Brasil 2008–2009 (2010).
[34] ASM Handbook Committee, *Properties and Selection: Nonferrous Alloys and Special-Purpose Materials* (ASM International, 2007). doi: 10.31399/asm.hb.v02.9781627081627
[35] D. Neumann, *Kinesiology of The Musculoskeletal System* (Elsevier B.V., 2010).
[36] D. S. Zlatanov, *Generalized Singularity Analysis of Mechanisms* (University of Toronto, 1998).
[37] O. Altuzarra, C. Pinto, R. Avilés and A. Hernández, "A practical procedure to analyze singular configurations in closed kinematic chains," *IEEE Trans. Robot.* **20**(6), 929–940 (2004).
[38] O. Altuzarra, O. Salgado, V. Petuya and A. Hernández, "Point-based Jacobian formulation for computational kinematics of manipulators," *Mech. Mach. Theory* **41**(12), 1407–1423 (2006).
[39] A. Hernández, O. Altuzarra, R. Avilés and V. Petuya, "Kinematic analysis of mechanisms via a velocity equation based in a geometric matrix," *Mech. Mach. Theory* **38**(12), 1413–1429 (2003).

Cite this article: R. S. Gonçalves and L. A. O. Rodrigues (2022). "Development of nonmotorized mechanisms for lower limb rehabilitation", Robotica **40**, 102–119. https://doi.org/10.1017/S0263574721000412